Available online at www.sciencedirect.com
ScienceDirect
Journal of Power Sources 164 (2007) 210–221
JOURNAL OF POWER SOURCES
www.elsevier.com/locate/jpowsour

A model for a vertical planar air breathing PEM fuel cell

B.P.M. Rajani, Ajit Kumar Kolar *

Heat Transfer and Thermal Power Laboratory, Department of Mechanical Engineering, IIT Madras, Chennai 600036, India

Received 23 July 2006; received in revised form 6 October 2006; accepted 6 October 2006
Available online 28 November 2006

Abstract

This paper presents a two-dimensional, steady state, single phase, non-isothermal and complete model for a vertical, fully planar, Air Breathing Proton Exchange Membrane Fuel Cell (AB-PEMFC) with hydrogen fuel supplied by forced convection at the anode. It is applied to a cell with an active area of 6 cm^2 operating at ambient atmospheric conditions of 23 °C and 20% relative humidity. The transport characteristics in terms of the velocity, and heat and mass transfer coefficients in the various components of the fuel cell are reported for several values of the operating current density. The effect of cathode height (1–5 cm) and operating atmospheric conditions (10–40 °C and 20–80% relative humidity), on the cell performance is also reported. Further, the applicability of the model to a non-planar AB-PEMFC is examined by comparison with available experimental data.

The average mass transfer coefficients for oxygen and water vapor at the cathode GDL surface are found to be of the order of 10^{-3} m s^{-1}. The operating current density is seen to substantially affect the variation of the local current density distribution and the cathode surface temperature along the height of the fuel cell as also the temperature variation across the MEA thickness. The maximum power density and the corresponding current density, herein defined as the optimum current density, are found to increase with decreasing height of the fuel cell, decreasing ambient temperature and increasing ambient relative humidity. However, the local cell temperature at high current densities is found to increase beyond the safe operating limits for short fuel cells. Comparison of the model predictions with available experimental data points to its applicability in the ohmic polarization zone of a non-planar cell. The cell performance at high current densities deteriorates due to mass transport limitation and electrolyte dehydration.

Keywords: Air breathing; Planar cathode; Model; Performance characteristics; Parametric study

1. Introduction

In conventional PEM fuel cells, the fuel (hydrogen or methanol) and the oxidant (air or oxygen) are supplied to the anode and the cathode, respectively, by forced convection through appropriately designed flow passages. Such fuel cells need auxiliary devices like fans, compressors, humidifiers, and mass flow controllers which occupy a considerable volume of space, add substantial weight and parasitic power, while increasing the cost of the complete fuel cell system. These requirements generally increase with increasing fuel cell capacity making the layout complex, maintenance difficult and operation involved. While large capacity fuel cell systems may not be substantially affected and may not be able to avoid this, the elimination of these auxiliary devices may be expected to benefit small capacity fuel cell systems, the benefit being greater for smaller systems. Thus, fuel cells which absorb one or both the reactants by natural convection have great potential in avoiding the use of auxiliary equipments and are ideally suited for low power applications. One could then refer to the fuel cells in which both the fuel and oxidant are taken in by free convection as "free breathing" or "passive", while those which take in only one reactant by free convection as "semi breathing". In particular, "air breathing" cells are those where only the air is absorbed by free convection at the cathode surface.

For a given fuel supply condition, the performance of these air breathing fuel cells, characterized by the operating cell voltage and current density range, maximum power density, and the optimum current density strongly depends on the rate of oxidant supply at the cathode surface. The oxidant supply is influenced by the free convection mass transfer coefficient at the cathode GDL surface which in turn is dependent on the cathode design and ambient operating conditions. Free convection has smaller heat and mass transfer coefficients when compared to

* Corresponding author. Tel.: +91 44 2257 4653; fax: +91 44 2257 0509.
E-mail address: kolar@iitm.ac.in (A.K. Kolar).

0378-7753/$ – see front matter © 2006 Published by Elsevier B.V.
doi:10.1016/j.jpowsour.2006.10.055

Nomenclature

a	activity
c_p	specific heat ($J\,kg^{-1}\,K^{-1}$)
D	diffusivity ($m^2\,s^{-1}$)
F	faraday's constant ($96485\,C\,mol^{-1}$)
h_m	mass transfer coefficient (ms^{-1})
I	current density ($A\,m^{-3}$)
I_0	exchange current density ($A\,m^{-3}$)
k_{eff}	effective thermal conductivity ($W\,m^{-1}\,K^{-1}$)
M	molecular weight ($kg\,mol^{-1}$)
n	no. of electrons transferred
nd	net drag coefficient
P	pressure ($N\,m^{-2}$)
R	universal gas constant ($8.314\,J\,mol^{-1}\,K^{-1}$)
RH	relative humidity
S	entropy ($J\,kg^{-1}\,K^{-1}$)
S_m	source term for continuity ($kg\,m^{-3}\,s^{-1}$)
S_{mom}	source term for momentum ($N\,m^{-3}$)
S_h	source term for energy ($W\,m^{-3}$)
S_i	source term for species ($kg\,m^{-3}\,s^{-1}$)
t	thickness (m)
T	temperature (K)
V	cell voltage (V)
Y	mass fraction

Symbols

α	net water transport coefficient
ρ	density ($kg\,m^{-3}$)
μ	viscosity ($m^2\,s^{-1}$)
β	permeability (m^2)
ε	porosity
ΔS	entropy change ($J\,mol^{-1}\,K^{-1}$)
η	activation overpotential (V)
λ	water content in the membrane
σ	conductivity ($S\,m^{-1}$)

Subscripts

a	anode
c	cathode
cat	catalyst
conc	concentration
gdl	gas diffusion layer
H_2O	water vapour
lim	limiting
mem	membrane
oc	open circuit
O_2	oxygen
w	water

forced convection, and thus, restricts the maximum obtainable current and power densities from the air breathing fuel cell. The potential application of AB-PEMFCs is therefore in small and portable appliances like watches, mobile phones, laptop computers, UPS systems and small decentralized energy applications, which need low to medium power capacities ranging from few milli Watts to several Watts [1–4]. In the recent past considerable interest has been shown by researchers in constructing AB-PEMFCs for investigation of their performance under various designs, in particular the cathode design, and operating conditions for proper operation and possible optimization. Both, passive Direct Methanol Fuel Cells and air breathing Hydrogen (H_2)-air fuel cells have been studied.

In particular, in the case of air breathing H_2-air fuel cells, various designs such as planar cathode, ducted cathode and ribbed cathode have been considered for research and development. An AB-PEMFC is considered to be planar if the cathode GDL has a perfectly planar surface without any protrusions or physical disturbances and completely open to atmosphere as shown in Fig. 1(a) for absorbing the required oxygen from air. However the ducted cathode AB-PEMFC as shown in Fig. 1(b) is the most frequently used design which consists of cathode ducts open to atmosphere at top and bottom. The ribbed cathode AB-PEMFC as shown in Fig. 1(c) has current collecting ribs on the cathode GDL which reduce the effective open area to the atmosphere. The reported literature is mainly focused on the experimental studies of cell performance and parametric distribution which is specific to certain operating conditions and the cell design [5–14], while the reported theoretical analysis [15–19] is limited to the analysis of multi-ducted non-planar cathode design.

Modeling of AB-PEMFCs differs from that of conventional (forced convection) fuel cells in an additional buoyancy term (due to both concentration and temperature difference) in the momentum equation. The unknown parameter of air flow rate due to free convection adds to the complexity of the model. It is therefore a challenging process and involves complex transport phenomena of multi-component, two-phase, multi-dimensional combined heat and mass transfer through porous medium coupled with electrochemical reactions.

To the best knowledge of the authors, Li et al. [15], Mennola et al. [16] and Ying et al. [17,18] are the only theoretical studies reported for vertical ducted cathode AB-PEMFCs while Rajani and Kolar [19] attempted to model vertical planar cathode AB-PEMFCs. Li et al. [15] treated the fuel cell cathode surface to be a plate and invoked the heat and mass transfer analogy in free convection to estimate approximately the current densities as a function of oxygen and water vapour mass fractions. The 2D steady state isothermal model developed by Mennola et al. [16] requires measured current density as input, and hence, can be treated as a semi-empirical mass transport model applicable only to a ducted cathode AB-PEMFC. Recently, Ying et al. [17] developed a 3D steady state, single phase, non-isothermal model for the complete AB-PEMFC with ducted cathode and simulated the effect of duct spacing on the fuel cell performance. They, however, did not report the numerical results at low current densities (<100 mA cm^{-2}), where the activation overpotential is significant.

The present authors are not aware of any reported models on planar air breathing fuel cells. As a first approximation, Rajani and Kolar [19] utilized standard similarity profiles for combined heat and mass transfer over a vertical plate and estimated the performance and parametric distributions in the vertical planar cathode AB-PEMFC with limited success. The available

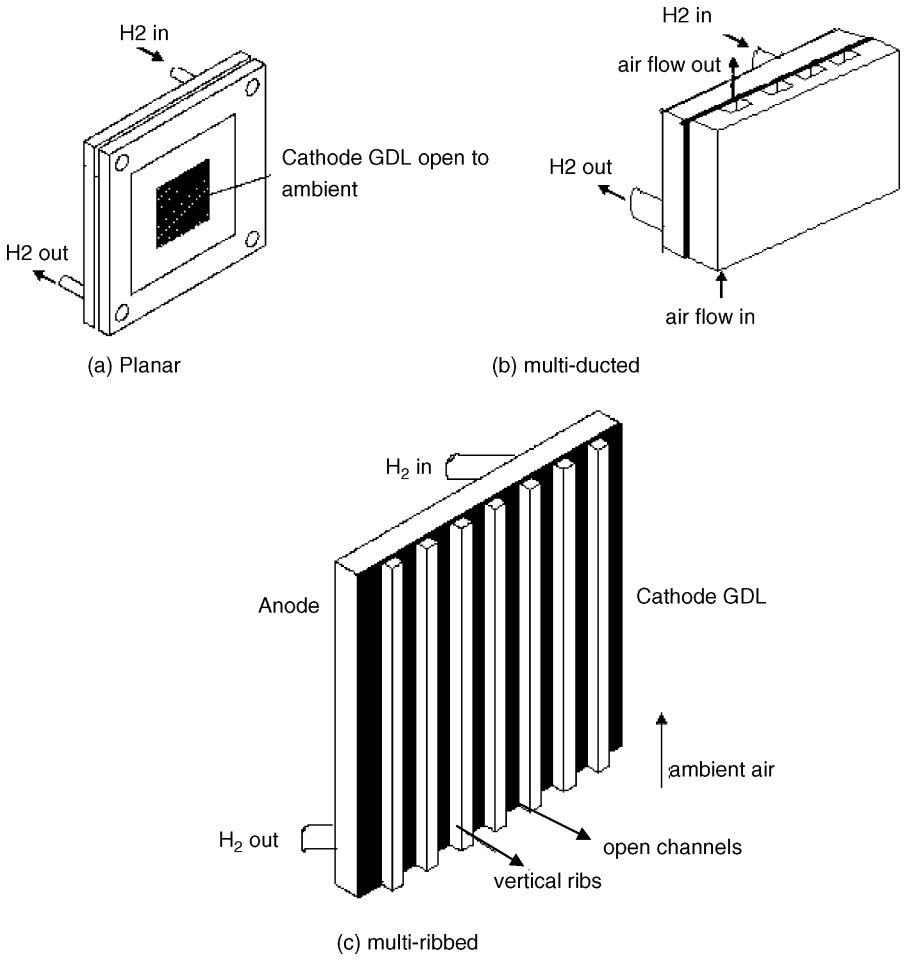

Fig. 1. Air breathing fuel cells.

theoretical studies predict only the polarization curve without giving the heat and mass transfer characteristics under different atmospheric conditions which are expected to influence the performance of the fuel cell.

The present study therefore aims at analyzing the performance of a vertical planar H_2-air AB-PEMFC under various operating conditions by using a 2D, steady state, single phase, non-isothermal and complete fuel cell model involving both flow and electrochemistry. It further describes the heat and mass transfer characteristics and presents the parametric effects.

2. Complete fuel cell model (CFCM)

2.1. Assumptions

The model is 2D (along the cell height and across the cell thickness perpendicular to the reactant flow direction) and is analyzed for the steady state conditions. The water generated and transported is assumed to be in vapour phase only and the cell is considered as non-isothermal. Gases are assumed to be ideal and ideal-gas mixing law is used for mixture properties like viscosity and thermal conductivity. The catalyst layer is considered to be very thin and is analyzed in 1D (along the height). The cell is vertically oriented and the anode flow passage is straight. The H_2 gas enters at the top and exits at the bottom of the anode flow passage transferring H_2 by forced convection.

2.2. Physical model

Fig. 2 (not to scale) presents the physical model for a vertical planar cathode fuel cell. It shows the complete single fuel cell structure that includes the membrane flanked by anode and cathode catalyst layers, gas diffusion layers (GDLs), anode flow duct and flow field plate together with an extended domain.

2.3. Mathematical model

The Complete Fuel Cell Model (CFCM) consists of three complementary sub-models: flow/transport sub-model, membrane sub-model and electrochemical sub-model. The flow/transport sub-model involves the solution of conservation equations of continuity, momentum, species and energy with appropriate source terms. The membrane sub-model involves the calculation of membrane characteristics like membrane proton conductivity and net water transport coefficient. The electrochemical sub-model involves the calculation of current density, overpotentials, voltage and power density.

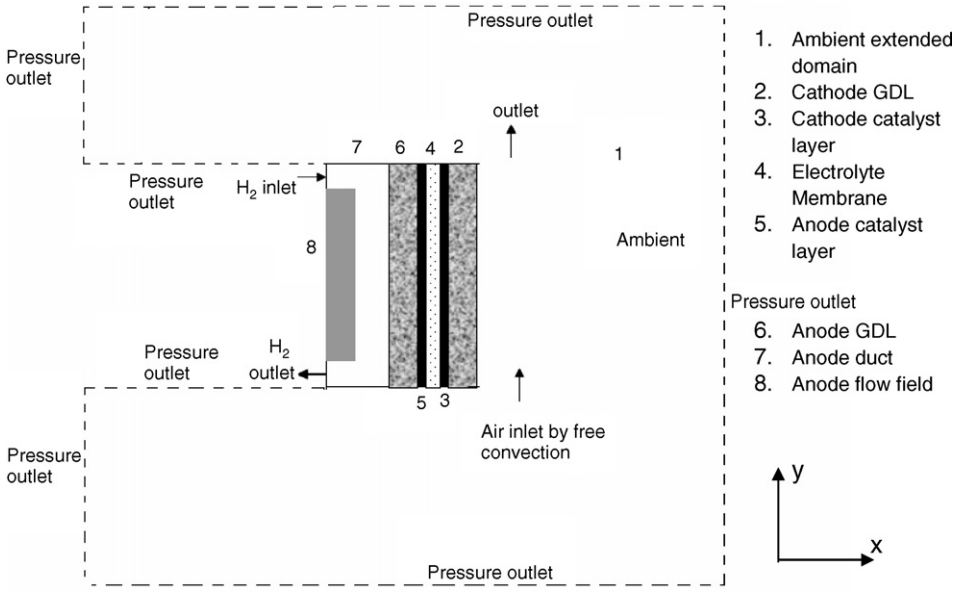

Fig. 2. Physical model for planar AB-PEMFC considered in CFCM.

2.3.1. Flow/transport sub model

The governing equations are based on the conservation of mass, momentum and energy for a 2D, steady state, single-phase case and include the convection, diffusion and the applicable source terms. Modeling of AB-PEMFCs differs from that of conventional fuel cells in that an additional buoyancy term (due to both concentration and temperature difference) appears in the momentum equation. The governing equations are as follows:

$$\text{Continuity}: \quad \nabla(\rho v) = S_{\mathrm{m}} \tag{1}$$

The source term for continuity is applicable only for the catalyst region.

$$\text{Anode catalyst layer}: \quad S_{\mathrm{m}} = -\frac{I}{2F}M_{\mathrm{H_2}} - \frac{\alpha I}{F}M_{\mathrm{H_2O}} \tag{2}$$

$$\text{Cathode catalyst layer}: \quad S_{\mathrm{m}} = -\frac{I}{4F}M_{\mathrm{O_2}} + \frac{(1+2\alpha)I}{2F}M_{\mathrm{H_2O}} \tag{3}$$

In other zones, i.e., in ducts, GDL and membrane, $S_{\mathrm{m}} = 0$.

$$\text{Momentum}: \quad \frac{1}{\varepsilon^2}\nabla(\rho v v) = -\nabla p + \frac{1}{\varepsilon}\nabla(\mu \nabla v) + \rho g + S_{\mathrm{mom}} \tag{4}$$

The source term is applicable only for porous medium where Darcy's viscous resistance term is included. Due to very low flow rates, the inertial loss is considered to be negligible. The source term is thus given by,

$$S_{\mathrm{mom}} = -\frac{\mu v}{\beta} \tag{5}$$

In other zones, i.e., in ducts and membrane, $S_{\mathrm{mom}} = 0$.

$$\text{Species}: \quad \nabla(\rho v Y_i) = -\nabla J_i + S_i \tag{6}$$

where species flux is given by:

$$\vec{J}_i = -\rho D_{i,m} \nabla Y_i \tag{7}$$

The source terms are applicable only to the catalyst layer and are as given below:

Hydrogen source term at anode catalyst layer :

$$S_{\mathrm{H_2}} = -\frac{I}{2F}M_{\mathrm{H_2}} \tag{8}$$

Water source term at anode catalyst layer :

$$S_{\mathrm{H_2O},a} = -\frac{\alpha I}{F}M_{\mathrm{H_2O}} \tag{9}$$

Oxygen source term at cathode catalyst layer :

$$S_{\mathrm{O_2}} = -\frac{I}{4F}M_{\mathrm{O_2}} \tag{10}$$

Water source term at cathode catalyst layer :

$$S_{\mathrm{H_2O},c} = \frac{(1+2\alpha)I}{2F}M_{\mathrm{H_2O}} \tag{11}$$

In other zones, i.e., ducts, GDL and membrane, $S_i = 0$

$$\text{Energy}: \quad \nabla(\rho c_{\mathrm{p}} v T) = \nabla(k_{\mathrm{eff}} \nabla T) + S_{\mathrm{h}} \tag{12}$$

S_{h} is the heat source term and is applicable at the cathode catalyst only and is given by:

$$S_{\mathrm{h}} = \left(-\frac{T\Delta S}{4F} + V_{\mathrm{act}}\right) I \tag{13}$$

In other zones, i.e., ducts, GDL and membrane, $S_{\mathrm{h}} = 0$

2.3.2. Membrane sub-model

The electrolyte membrane conductivity, 'σ_{m}' is an important property that depends on the water content of the membrane,

'λ'. It is always desired to maintain the membrane under fully humidified condition in a PEMFC to obtain the highest 'λ'. The net water content in the membrane is the resultant of water transport by three main processes—(i) the electro-osmotic drag due to protons from anode to cathode, (ii) the back diffusion from cathode to anode due to concentration difference and (iii) the net flow of water due to the pressure difference. In the present model, the water transport due to pressure difference is not considered, as the operating pressures are atmospheric. Springer et al. [20] proposed a 1D model for calculating the membrane characteristics as given below:

The water content in the membrane (λ) is based on the activity of water and can be expressed as:

$$\lambda = 0.043 + 17.8a - 39.85a^2 + 36a^3, \quad \text{if } 0 < a \leq 1 \tag{14}$$

$$\lambda = 14 + 1.4(a-1), \quad \text{if } 1 < a \leq 3 \tag{15}$$

where, activity at anode and cathode:

$$a = \frac{X_{H_2O}P}{P_{sat}} \tag{16}$$

The concentration of water at catalyst–membrane interface:

$$C_w = \frac{\rho_{m,dry}}{M_{m,dry}}\lambda \tag{17}$$

Eq. (17) is applied for both anode ($C_{w,a}$) and cathode ($C_{w,c}$) catalyst–membrane interfaces where membrane density ($\rho_{m,dry}$) and equivalent weight of membrane ($M_{m,dry}$) are considered to be 2000 kg m^{-3} and 1.1 kg mol^{-1}, respectively. The net drag coefficient (nd) is defined as the number of water molecules dragged per proton from anode to cathode and is expressed as a function of water content as:

$$\text{nd} = \frac{2.5\lambda}{22} \tag{18}$$

The net water transport coefficient (α) is given by:

$$\alpha = \text{nd} - \left(FD_w\frac{C_{w,c} - C_{w,a}}{It_{cat}\,t_{mem}}\right) \tag{19}$$

where water diffusion coefficient in membrane, D_w (m^2 s^{-1}) is given as:

$$D_w = 5.5 \times 10^{-11}\,\text{nd}\exp\left(2416\left(\frac{1}{303} - \frac{1}{T}\right)\right) \tag{20}$$

The membrane proton conductivity is strongly dependent on its water content and is expressed as:

$$\sigma_m = [0.514\lambda - 0.326]\exp\left[1268\left(\frac{1}{303} - \frac{1}{T}\right)\right] \tag{21}$$

The present analysis calculates the above membrane properties and uses them further with the flow model for the prediction of the local parametric distribution.

2.3.3. Electrochemical sub-model

The local current density is calculated using Butler-Volmer Eq. (22) and the exchange current density (I_0) is calculated as a function of temperature Eq. (23), as follows:

$$I = I_0\left(\frac{C_{O_2,cat/mem}}{C_{O_2,ref}}\right)\left(\exp\left(\frac{\alpha_a FV_{act}}{RT}\right) - \exp\left(\frac{-\alpha_c FV_{act}}{RT}\right)\right) \tag{22}$$

$$I_0 = I_{o(T_{ref})}\left(\exp\left(\frac{\Delta E}{R}\left(\frac{1}{T_{ref}} - \frac{1}{T}\right)\right)\right) \tag{23}$$

where ΔE—activation energy is 72,000 J mol^{-1}, T_{ref} used is 353 K (80 °C), I_0 at 353 K is 10 A m^{-3} and $C_{O_2,ref}$ is 3.39 mol m^{-3} [21].

The open circuit potential is considered as a function of temperature as given by Parthasarathy et al. [22],

$$V_{oc} = 0.0025T + 0.2329 \tag{24}$$

The voltage losses considered in calculating the net cell voltage (V_{cell}) include the activation overpotential, ohmic losses (in membrane, GDL and current collectors), and the concentration losses based on limiting current density. The net cell voltage is hence given by,

$$V_{cell} = V_{oc} - V_{act} - \frac{It_{cat}t_{mem}}{\sigma} - \frac{It_{cat}t_{gdl}}{\sigma_{gdl}} - \frac{It_{cat}t_{flow\_plate}}{\sigma_{flow\_plate}} + V_{conc} \tag{25}$$

The activation overpotential is the voltage loss associated in overcoming initial activation barrier. The ohmic losses are the IR losses associated with the resistance offered to the flow of electrons and are dependent on the proton conductivity of the membrane and the electrical conductivity of GDL, current collectors and the end plates. The concentration overpotential (V_{conc}) is associated with the voltage loss due to mass transport limitation which can be significant and contributes to the decrease in the cell voltage. For air breathing fuel cells, the concentration overpotential is mainly associated with the oxidant availability, and hence, it is defined based on the limiting current density and is given by,

$$V_{conc} = \frac{RT}{4F}\left(\ln\left(1 - \frac{It_{cat}}{I_{lim}}\right)\right) \tag{26}$$

where the limiting current density, I_{lim} is the maximum current density that can be derived from a fuel cell and is given by,

$$I_{lim} = \frac{4FC_{O_2,\infty}}{(t_{gdl}/D_{O_2,eff}) + (1/h_{m,i})} \tag{27}$$

The local mass transfer coefficient for the species i, $h_{m,i}$ used in the above expression is at the GDL surface and is calculated using,

$$h_{m,i} = \frac{D_{ij}(\partial Y_i/\partial x)\big|_{GDL}}{(Y_{i,GDL} - Y_{i,\infty})} \tag{28}$$

$Y_{i,GDL}$ is mass fraction at GDL surface, $Y_{i,\infty}$ is the mass fraction in the ambient.

2.4. Boundary conditions

2.4.1. Anode

The anode inlet conditions are specified with the input mass fractions, temperature and pressure of H_2.

$$\text{At anode inlet}: \quad Y_{H_2} = Y_{H_2,\text{in}}; \qquad T_{H_2} = T_{\text{in}}; \qquad P_{H_2} = P_{\text{in}} \tag{29}$$

$$\text{At anode outlet}: \quad \frac{\partial Y_i}{\partial x} = 0 \tag{30}$$

2.4.2. Cathode

At cathode inlet, cathode outlet, GDL surface and GDL-catalyst interface, boundary condition specified is of 'interior' type. An interior boundary condition is taken as internal face zone and does not require any additional input. It calculates by applying flux balance.

The remaining edges are specified as walls which means

$$Y_i = 0, \qquad v_i = 0. \tag{31}$$

At extended domain, mass fractions and pressure are specified to that of the undisturbed ambient.

$$Y_i = Y_\infty; \qquad P = P_\infty \tag{32}$$

2.5. Solution methodology

The physical model (Fig. 2) is created and meshed using GAMBIT. An extended domain is considered around the fuel cell such that the pressure at the boundaries is equal to that of the undisturbed atmosphere. The dimensions of the extended domain are varied and are finally fixed at values for which the computation time is reduced and with no compromise on the accuracy. Fluent 6.1 incorporated with User Defined Functions (UDFs) is used as a platform for computation. The solution algorithm is as shown in Fig. 3. The computation procedure follows a single domain or unified approach for solving the conservation equations of continuity, momentum, energy and species governing the entire domain of interest, i.e., GDL, catalyst layer and extended domain with relevant source terms accounting with in the cell. The hydrogen inlet operating conditions (mass flow rate, temperature, pressure and relative humidity) and the ambient conditions (ambient temperature and relative humidity) are given as input parameters.

Table 1
Reference diffusivities used in the model

	($m^2\ s^{-1}$)
$D_{H_2-H_2O}$	9.15e-5
$D_{H_2-O_2}$	7e-5
$D_{O_2-N_2}$	2.2e-5
$D_{H_2-N_2}$	6.8e-5
$D_{O_2-H_2O}$	2.82e-5
$D_{H_2O-N_2}$	2.56e-5

The solution starts with a specified value of activation overpotential and with initial guessed values of mass fractions in the computation domain viz., catalysts, GDL, and extended domain. The governing equations are solved using Finite Volume Method (FVM) and the solution is based on pressure correction method and uses SIMPLE algorithm [23]. The second order upwind differencing scheme is used for momentum, species and energy equations. The mixture is considered to be ideal gas and the effective properties of viscosity and thermal conductivity are based on ideal-gas mixing law. Multi-component diffusion is considered and the effective diffusivity of the mixture is calculated at different temperatures and pressures based on the experimental reference diffusivities reported by Guvelioglu and Stenger [24] and are given in Table 1. The solution is iterated till the required convergence of average current density, cell voltage, species concentrations, velocity and temperature is obtained.

This method is repeated for different activation overpotential values in order to obtain the overall polarization curve of the cell. The activation overpotential values start from 0.1 V and increase initially in steps of 0.05 or 0.1 depending on the current densities obtained. At high current densities, it is increased in steps of 0.002–0.005 as the variation in activation polarization at high current densities, i.e., in ohmic and concentration overpotential zones is not substantial. The model can also be modified to take either an average current density or cell voltage

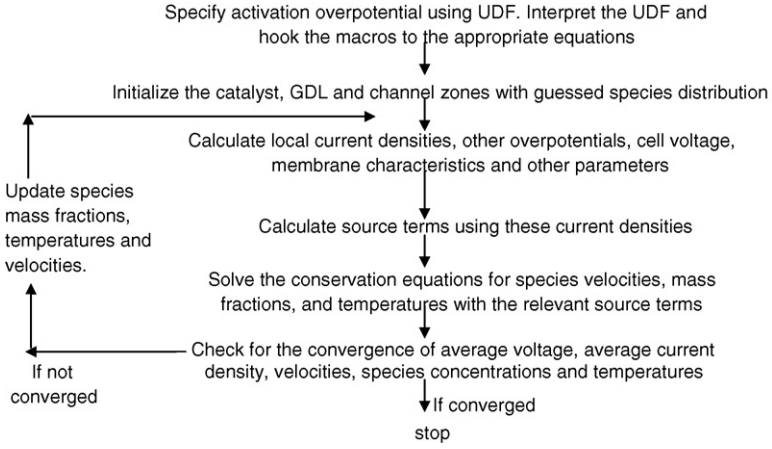

Fig. 3. Solution algorithm for CFCM.

as input parameters instead of activation overpotential. However, the current density or cell voltage input method involves an additional inner loop for solving the activation overpotential as both the quantities (current density and activation overpotential or cell voltage and activation overpotential) are interdependent on each other. Incorporation of an additional loop complicates the analysis, and hence, the present simpler model of considering the activation overpotential as an input is used. Further information regarding the meshing, solving and post processing can be found in reference [25] and Kumar and Reddy [26] is the recent article published on the analysis of conventional fuel cells using Fluent.

3. Results and discussion

3.1. Heat and mass transfer characteristics

The heat and mass transfer characteristics involve the analysis of the distribution of species concentrations, temperature and mass transfer coefficients in all the components of a fuel cell *viz.*, cathode surface, GDL, catalyst layer and membrane. In addition to this, the transport characteristics involve the study of velocities and local current densities. This study would help in understanding the physics involved and further in identifying the practical operating conditions. Figs. 4–11 illustrate the heat and mass transfer characteristics in a single planar fuel cell of design and operating conditions same as that of Hottinen et al. [12] as given in Table 2.

3.1.1. Local variation at medium and high current densities

Figs. 4–7 show the velocity, species concentration and temperature profiles at medium and high average current densities of 258 mA cm^{-2} and 926 mA cm^{-2}, respectively.

Fig. 4(a) and (b) show the resultant air velocity profiles at the cathode GDL surface. At both the current densities, an increase in the boundary layer thickness together with the corresponding increase in the maximum velocity can be observed along the height indicating the upward buoyancy induced in the air flow. The maximum velocity at the exit can also be found to increase with increase in the current density. However, at both the current densities, the maximum resultant velocity is observed to shift towards cathode GDL surface after a height of about 2 cm from the inlet. A possible reason might be the end effect at the exit where the fresh atmospheric conditions exist. Fig. 5 illustrates the variation of mass fractions of O_2 and H_2O along the cathode GDL surface. The decrease in the oxygen mass fraction and the corresponding increase in the water vapour mass fraction can be clearly observed along the fuel cell height and also at two different current densities. The consumption and production of species is more at high current densities when compared to that at low current densities.

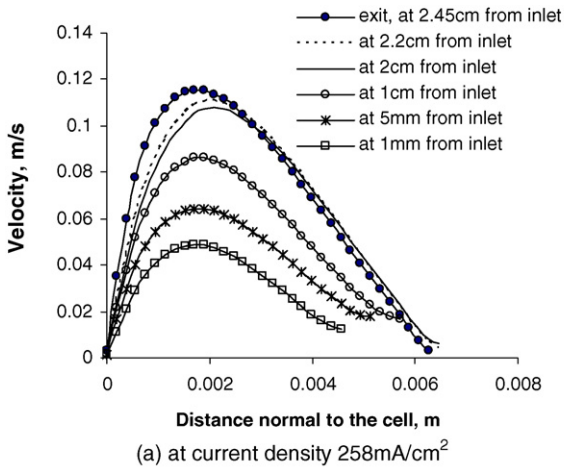

(a) at current density 258mA/cm^2

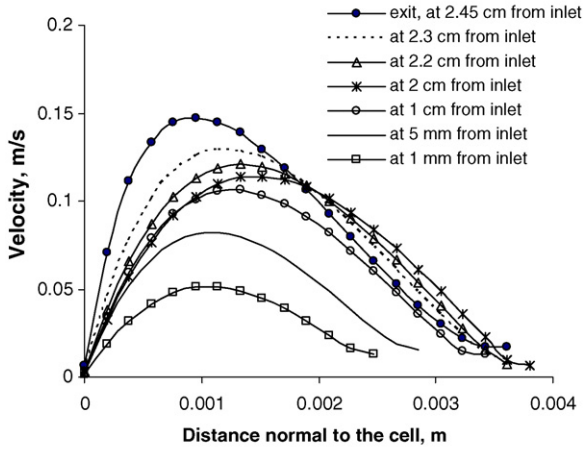

(b) at current density 926mA/cm^2

Fig. 4. Resultant air velocity profiles at the cathode GDL surface.

The variation of local current density and the cathode GDL surface temperature along the fuel cell height is shown in Fig. 6. The O_2 mass fraction is high but the air velocity is low at the inlet when compared to that at the exit. Due to this, there is a slight increase in the current density close to the inlet. Further, the increase in the concentration boundary layer thickness along the cathode GDL surface increases the resistance offered to the diffusion of the gas. Hence, the local current density decreases after a certain height. The variation in local

Table 2
Design and operating parameters of Hottinen et al. [12] experiments used for comparison of planar cathode model

Design parameters	
Cell height	2.45 cm
Cathode GDL thickness	1.5 mm
Membrane thickness	50.8 μm
H_2 duct cross section	1 mm × 1 mm
Permeability of catalyst layer	1.76e-12 m^2
Active area	6 cm^2
Anode GDL thickness	420 μm
Catalyst layer thickness	10 μm
Permeability of GDL	1.8e-18 m^2
Operating parameters	
Ambient and H_2 temp	23 °C
Rel. Humidity of H_2	0% (dry)
Cathode pressure	1 atm. (abs.)
Ambient Rel. Humidity	20%
H_2 flow rate	9.3e-10 kg s^{-1}
Anode pressure	1 atm. (abs.)

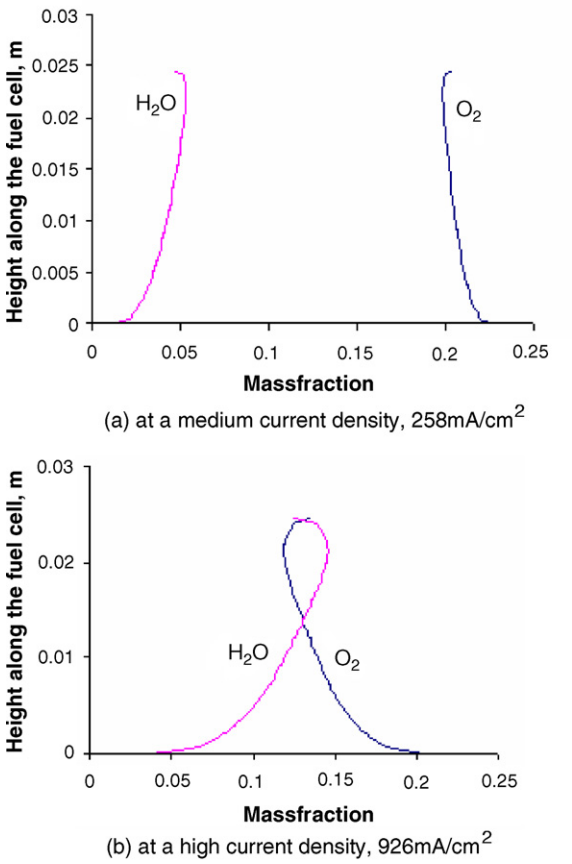

Fig. 5. Variation of O_2 and H_2O mass fraction on the surface of the cathode GDL along the height of fuel cell.

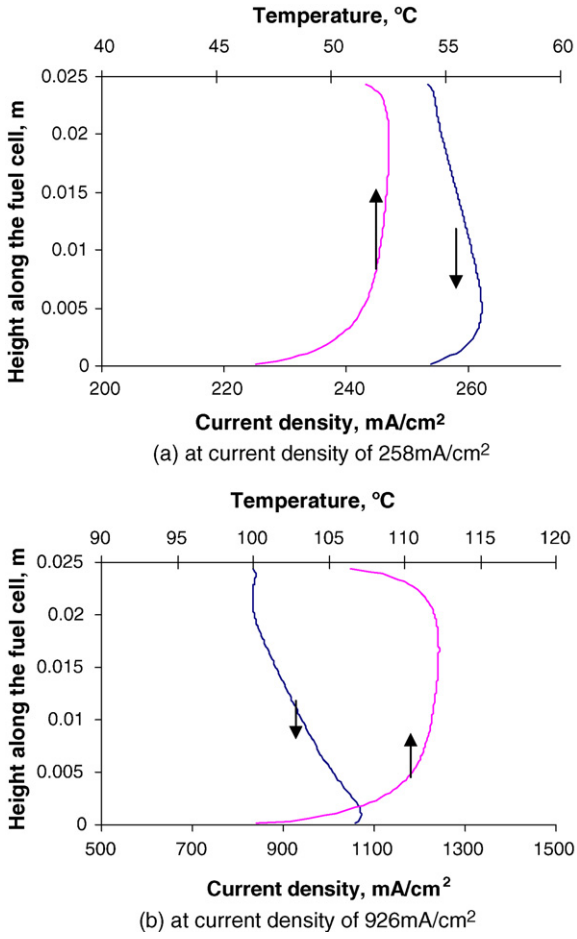

Fig. 6. Variation of local current density and the cathode GDL surface temperature along the height of the fuel cell.

surface temperature follows that of local current density as the heat produced in the electro-chemical reaction is dependent on the operating current density. The variation in surface temperature is observed to be about 5 °C for medium current densities and about 10 °C for high current densities, which is significant enough to confirm the non-isothermality of the single planar AB-PEMFC.

Fig. 7 illustrates the temperature variation across MEA which includes membrane sandwiched between catalyst coated anode and cathode GDLs. The maximum temperature across MEA can be observed at the cathode catalyst–electrode–electrolyte interface (three-phase boundary) as it is the active reaction site for complete fuel cell reaction, and hence, the heat generation. The temperature drop is high in the cathode GDL when compared to that in the anode GDL. The cathode GDL surface has a free convective atmospheric air which has low heat transfer coefficient when compared to the forced convective heat transfer coefficient of H_2 at the anode GDL surface. In addition to the difference in the convective heat transfer, the GDLs also differ in the thickness. The cathode GDL is thicker than that of the anode. The temperature gradient in the cathode GDL is found to be high at positions close to the inlet and is low near exit. This difference points to the effect of heat transfer coefficients and heat transfer on both sides (anode and cathode) along the height of the fuel cell. The temperature variation across MEA is about 3 °C for medium current density and is about 7 °C for high current density indicating that at high current densities, the temperature variation across MEA is substantial. Thus, the cell can be considered to be isothermal at low current densities and should be considered as non-isothermal at high current densities.

3.1.2. *Comparison at different current densities*

Figs. 8–11 compare the mass transfer coefficients, O_2 concentration, catalyst layer temperature and local current density distribution for a range of current densities from 143 mA cm^{-2} to 926 mA cm^{-2}.

Fig. 8 illustrates the local O_2 mass transfer coefficients at the cathode GDL surface for four different current densities. The local mass transfer coefficients are found to be of the order of 10^{-3} m s^{-1} with highest value at the bottom edge of the fuel cell and are observed to decrease with height along the cathode surface. Further, the increase in the mass transfer coefficients can be clearly observed with increase in the current density indicating the increase in the O_2 diffusion fluxes. Another important observation is that the deviation at the exit is predominant at high current densities when compared to that at low current densities.

The decrease in the mass transfer coefficient represents the decrease in the diffusive mass flux which in turn decreases the local current density. Fig. 9 shows the variation of local current densities at different average current densities. It can be

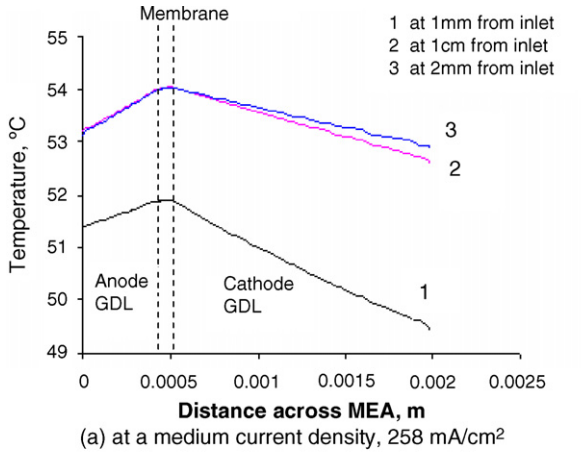

(a) at a medium current density, 258 mA/cm²

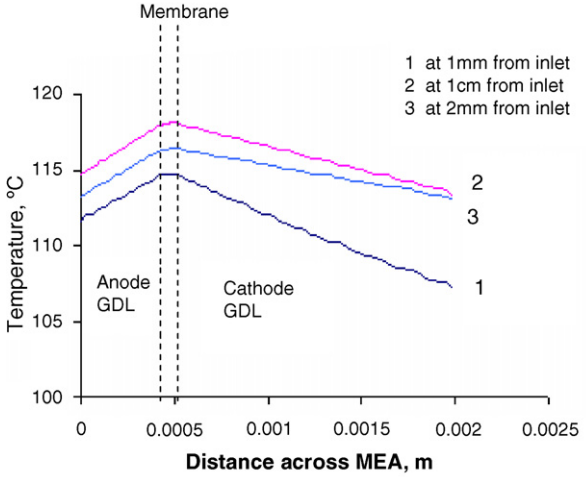

(b) at a high current density, 926mA/cm²

Fig. 7. Temperature variation across MEA.

observed that the variation is significant at high current densities and is not substantial at low current densities. This is due to the huge variation in the O_2 mass fractions at high current densities as shown in Fig. 10. The catalyst layer temperature depends on the operating current density, and hence, its variation is also substantial at high current densities as shown in Fig. 11. The catalyst layer temperature variation along the fuel cell height is found to be about 10 °C at high current densities where as it is about 4 °C at low current densities. This confirms the fact that a non-isothermal model is essential to predict the performance of the fuel cell especially at high current densities.

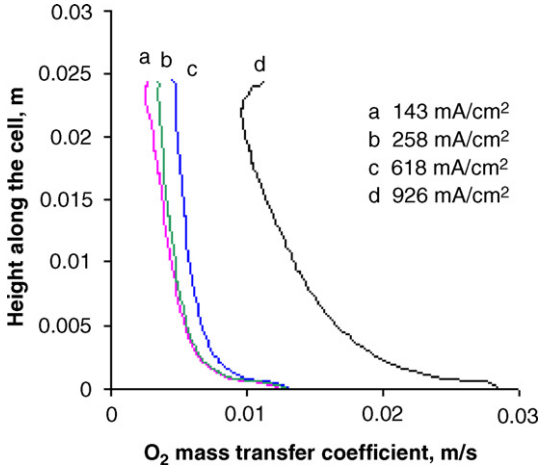

Fig. 8. Variation of O_2 mass transfer coefficients along the height of the fuel cell.

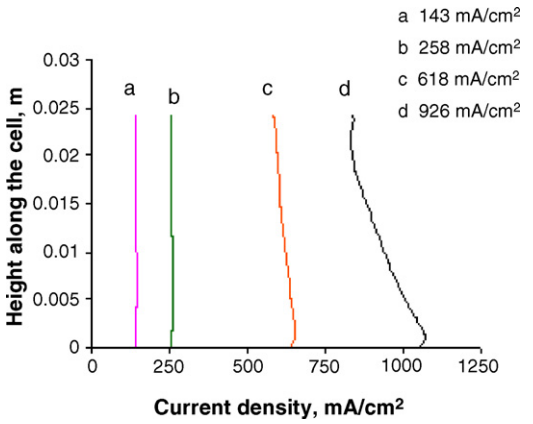

Fig. 9. Variation of local current density along the height of the fuel cell.

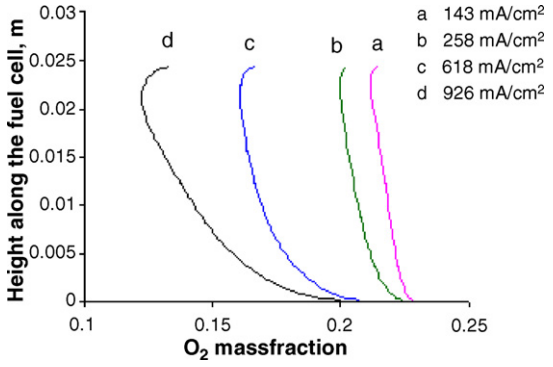

Fig. 10. Variation of O_2 mass fraction along the height of the fuel cell.

3.2. Parametric effects

The parameters considered for planar cathode AB-PEMFC are the fuel cell height and the atmospheric conditions.

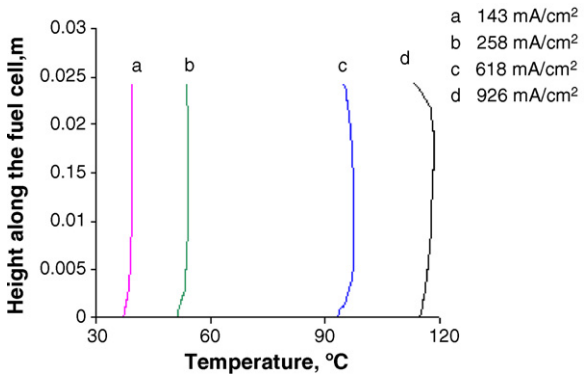

Fig. 11. Variation of catalyst layer temperature along the height of the fuel cell.

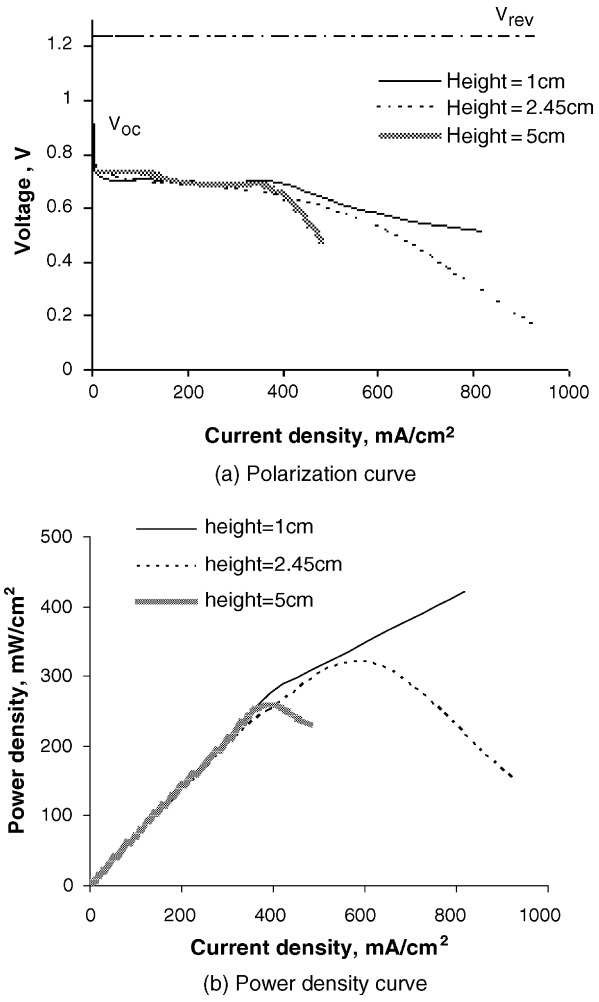

Fig. 12. Effect of fuel cell height on planar cathode AB-PEMFC performance.

3.2.1. Effect of fuel cell height

The fuel cell heights considered are 1 cm (short), 2.45 cm (medium) and 5 cm (tall) while keeping the active area unchanged at 6 cm^2. Fig. 12(a) and (b) illustrate the comparison of polarization and power density curves, respectively. It can be observed that there is no significant difference in the voltage and power density at low operating current densities. However, the maximum power density attained is observed to increase with decrease in the fuel cell height. Further, the operating current density range and the optimum current density (corresponding to the maximum power density) are also found to increase with decrease in the fuel cell height.

The improvement in the performance characteristics for the short fuel cell in the present study can be explained in terms of the boundary layer effects on the three polarization effects, namely, concentration overpotential, ohmic overpotential, and activation overpotential. The free convection boundary layer thicknesses on the vertical cathode surface (the velocity boundary layer δ_v, the thermal boundary layer δ_t, the concentration boundary layer δ_c) increase gradually along the fuel cell height resulting in a decrease in the velocity, temperature and concentration gradients at the surface. This in turn results in the increased resistance offered to the transfer of heat and oxidant between the cathode surface and the ambient air. Hence, the average heat and mass transfer coefficients will be high for short cells compared to the tall cells.

High mass transfer coefficient for oxygen transfer implies low concentration overpotential for short fuel cells resulting in some improvement in their performance. In the present study, the concentration overpotential at a current density of about 390 mA cm^{-2} is observed to be 0.684 mV for the short 1 cm fuel cell compared to 1.07 mV for the tall 5 cm fuel cell.

The short fuel cell, with its higher average heat transfer coefficient has a higher heat transfer rate, surface area being held constant as that of the tall cell, and hence, a better cooling effect. This implies that for the same operating current density (and hence, for the same amount of heat generation in the fuel cell), the short cell will be at a lower temperature. Lower the cell temperature, better the hydration state and higher the protonic conductivity of the membrane. Thus, the ohmic overpotential is low for short cells further leading to their improved performance. In the present study, the average cell temperatures are observed to be 88 °C and 50 °C for the 5 cm and 1 cm high fuel cells, respectively, at a current density of about 390 mA cm^{-2}. The corresponding ohmic voltage losses for a 5 cm and 1 cm high fuel cells are observed to be 0.198 V and 0.021 V.

The activation overpotential varies logarithmically with cell temperature and is high at low temperatures. The cell temperature is low for short cells, and hence, their activation overpotential is high. In the present case, the activation overpotential is about 273 mV for the short 1 cm fuel cell and 261 mV for the tall 5 cm fuel cell.

The combined effect of decreased ohmic and concentration overpotentials and the increased activation overpotential results in the short fuel cell performing better than the tall fuel cell. While this observation holds good in the present range of experiments, it is expected that the physical explanation can be applied to other experimental conditions and appropriate conclusions drawn.

Another important observation from the heat transfer analysis is that the local cell temperatures at high current densities exceeded the operating temperature limit of 100 °C. It is observed that for a 1cm high fuel cell, the cell temperature has crossed 120 °C at current densities of about 600 mA cm^{-2}. This may imply the inadequacy of free convective heat transfer under these conditions. Thus, despite better performance in terms of the operating current density range and power density for a short fuel cell, it is advisable to operate it at low current densities to ensure safe operating temperature limits.

In summary, it can be inferred from the above discussion that the shorter the cell the better the performance. In addition to this, one should also consider the practical and allowable operating current densities and the cell temperatures corresponding to the particular fuel cell height.

3.2.2. Effect of atmospheric conditions

The atmospheric operating conditions are not steady over the day and the AB-PEMFC gets subjected to the dynamic atmospheric conditions. It is therefore required to study the behavior of the AB-PEMFC under normal range of atmospheric condi-

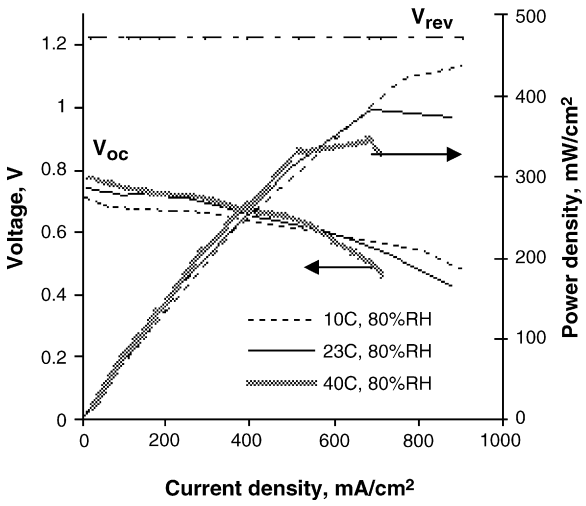

Fig. 13. Effect of atmospheric temperature on planar cathode AB-PEMFC Performance.

tions. The present study includes low, medium and high values of atmospheric temperatures (10 °C, 23 °C and 40 °C) and relative humidities (20%, 50% and 80%). Figs. 13 and 14 illustrate the effect of atmospheric temperature (at 80%RH) and relative humidity (at 40 °C), respectively, on the performance of planar AB-PEMFCs operating under similar design conditions.

It can be observed from Fig. 13 that, at low current densities, the decrease in the activation overpotential with increase in temperature hardly affected the power density indicating that at low current densities, the temperature has no significant effect on the power density. However, the maximum power density is observed to decrease with increase in temperature. The maximum power density at 10 °C is about 20% higher when compared to that at 40 °C. It is observed from the heat transfer analysis that the cell temperature attained at a current density of 600 mA cm^{-2} is 107 °C at an ambient temperature of 40 °C and that at an ambient of 10 °C, the cell temperature is 70 °C. It is therefore clear that the fuel cell operating at 40 °C could not operate at much higher current densities as it exceeds the safe operating temperature limit of 100 °C, and hence, the phenomenon of membrane dehydration is prone to occur. Thus, the optimum current density increases with decrease in atmospheric temperature. In addition to this, the reduction in the free convection air flow due to reduced temperature gradients limit the power density and current densities for fuel cells operating at high atmospheric temperatures.

Fig. 14 illustrates the effect of atmospheric relative humidity on fuel cell performance. It can be observed that at low current densities, the difference in the activation drop is negligible with change in the atmospheric relative humidity. However, at high current densities, a slight improvement in the power density is observed with increase in relative humidity and is due to the net increase in the membrane moisture content, and hence, the membrane conductivity. Thus, it can be observed that the effect of relative humidity on fuel cell performance is less significant when compared to that of atmospheric temperature.

Hence, it can be concluded from the above discussion that an effective performance can be achieved from a planar cathode AB-PEMFC of approximately 2–3 cm height operating at atmospheric conditions of low temperatures and high relative humidities.

3.3. Comparison with published experimental data

In the absence of experiments on a fully planar cathode cell in the literature, the present 2D planar CFCM is tested for its applicability to non-planar cathode cells. The experimental data of Hottinen et al. [12] on a vertical multi-ribbed cathode (non-planar cathode) AB-PEMFC with design and operating parameters as given in Table 2 is used for comparison. To facilitate a meaningful comparison, the ohmic resistance offered by the ribs of the non-planar cathode of Hottinen et al. [12] is incorporated in the total ohmic resistance of the planar model calculations. Fig. 15 illustrates the comparison.

The polarization plot is such that it can be approximately sub-divided into three zones: zone I (activation overpotential zone from 0 to 50 mA cm^{-2}), zone II (ohmic overpotential zone from 50 to 800 mA cm^{-2}) and zone III (concentration overpoten-

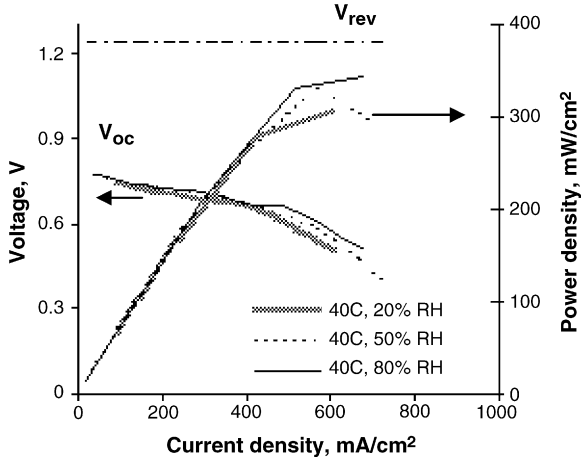

Fig. 14. Effect of atmospheric RH on planar cathode AB-PEMFC performance.

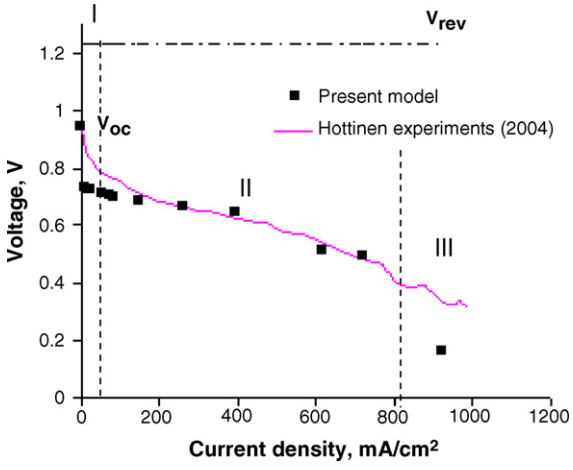

Fig. 15. Comparison of present CFCM predictions with Hottinen et al. [12] experiments on ribbed cathode AB-PEMFC.

tial zone for current densities above 800 mA cm^{-2}). The present model slightly under-predicts the voltages in the activation overpotential zone. This deviation can be attributed to the difference in the physical structure of the present cathode design with that of the actual experimental model. Some of the contributing factors can also be the anode duct shape which is considered to be a straight duct in the present model when compared to the actual z-type flow field in the experiments. Moreover, the effect of ribs and channels are eliminated for flow calculations and the surface is considered to be completely planar.

Despite these limitations in the zone I, the present model predictions are in good agreement with experimental data in zone II probably due to the predominant effect of ohmic overpotential which varies almost linearly with current density. In the concentration overpotential zone (zone III), the sudden drop in the voltage as predicted by the model at around 800 mA cm^{-2} is also observed experimentally. This may be attributed to the combined effect of the insufficient supply of the reactants at the reaction site and the membrane dehydration.

Thus, it can be concluded, that the present CFCM for fully planar cathode is also applicable to a multi-ribbed cathode AB-PEMFC only in the ohmic overpotential zone with little error.

4. Conclusions

The prediction of a 2D, steady state, non-isothermal, single phase, complete PEMFC model for a fully planar cathode air breathing fuel cell is presented, perhaps for the first time to the best knowledge of the authors. Based on the present model predictions, the average mass transfer coefficients for a planar AB-PEMFC are found to be of the order of 10^{-3} m s^{-1} with ambient conditions as the reference. The variations in parameters like current density, mass fractions and temperature are substantial at high current densities when compared to that at low current densities. The cell temperature variation at high current densities is found to be about 10 °C along the fuel cell height and about 7 °C across the MEA indicating the non-isothermality of the fuel cell. The current density range and the maximum power densities are observed to increase with decrease in the fuel cell height. The atmospheric temperature is found to have significant effect on fuel cell performance while the effect of atmospheric RH is observed to be negligible. The maximum power density is found to decrease by about 20% with about 30 °C increase in atmospheric temperature. Based on the present parametric study on a 6 cm^2 cell, it can be inferred that the acceptable power density and current density can be achieved by an air breathing fuel cell with short cell operating at atmospheric conditions of low temperatures and high relative humidities. In addition to the above, the present planar model is found to predict the performance in the ohmic overpotential zone of a non-planar cathode AB-PEMFC with little error.

References

[1] D. Jollie, Fuel Cell Today (2004).
[2] M. Daugherty, S. Hoffman, Fuel Cells Bull. 3 (2000) 10–13.
[3] C.K. Dyer, J. Power Sources 106 (2002) 31–34.
[4] A. Heinzel, C. Hebling, M. Muller, M. Zedda, C. Muller, J. Power Sources 105 (2002) 250–255.
[5] D. Chu, R. Jiang, J. Power Sources 83 (1999) 28–133.
[6] M. Noponen, T. Mennola, M. Mikkola, T. Hottinen, P. Lund, J. Power Sources 106 (2002) 304–312.
[7] T. Hottinen, M. Noponen, T. Mennola, O. Himanen, M. Mikkola, P. Lund, J. Appl. Electrochem. 33 (2003) 265–271.
[8] A. Schmitz, M. Tranitz, S. Wagner, R. Haln, C. Hebling, J. Power Sources 118 (2003) 162–171.
[9] R. Hahn, S. Wagner, A. Schmitz, H. Reichl, J. Power Sources 131 (2004) 73–78.
[10] T. Hottinen, M. Mikkola, P. Lund, J. Power Sources 129 (2004) 68–72.
[11] T. Mennola, M. Noponen, T. Kallio, M. Mikkola, T. Hottinen, J. Appl. Electrochem. 34 (2004) 31–36.
[12] T. Hottinen, O. Himanen, P. Lund, J. Power Sources 138 (2004) 205–210.
[13] F. Jaouen, S. Haasl, W.V. Wijngaart, A. Lundblad, G. Lindbergh, G. Stemme, J. Power Sources 144 (2005) 113–121.
[14] P.W. Li, S.P. Chen, M.K. Chyu, J. Power Sources 140 (2005) 311–318.
[15] P.W. Li, T. Zhang, Q.M. Wang, L. Schaefar, M.K. Chyu, J. Power Sources 114 (2003) 63–69.
[16] T. Mennola, M. Noponen, M. Aroneimi, T. Hottinen, M. Mikkola, O. Himanen, P. Lund, J. Appl. Electrochem. 33 (2003) 979–987.
[17] W. Ying, Y.J. Sohn, W.Y. Lee, J. Ke, C.S. Kim, J. Power Sources 145 (2) (2005) 563–571.
[18] W. Ying, T.H. Yang, W.Y. Lee, J. Ke, C.S. Kim, J. Power Sources 145 (2) (2005) 572–581.
[19] B.P.M. Rajani, A.K. Kolar, Proceedings of International Conference on Electrochemical Power Systems (ICEPS-2), Hyderabad, India, B-25, 2004.
[20] T.E. Springer, T.A. Zawodzinski, S. Gottesfeld, J. Electrochem. Soc. 138 (8) (1991) 2334–2342.
[21] D.M. Bernardi, M.W. Verbrugge, J. Electrochem. Soc. 139 (1992) 2477–2490.
[22] A. Parthasarathy, S. Srinivasan, A.J. Appleby, J. Electrochem. Soc. 139 (1992) 2530–2537.
[23] S.V. Patankar, Numerical heat transfer and fluid flow, McGraw Hill, New York, 1980.
[24] G.H. Guvelioglu, H.G. Stenger, J. Power Sources 147 (1/2) (2005) 95–106.
[25] http:www.fluent.com.
[26] Atul Kumar, R.G. Reddy, J. Power Sources 155 (2006) 264–271.